PAPER

Check for updates

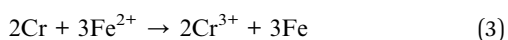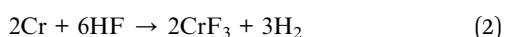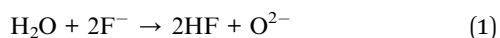# Electrolytic reduction of CrF₃ and Cr₂O₃ in molten fluoride salt

Nan Ji,[a] Fangling Jiang[*b] and Hao Peng ![ORCID] [*a]

The electrochemical behavior of Cr^{3+} in molten LiF–NaF–KF (46.5 : 11.5 : 42 mol%) (FLiNaK) was studied by cyclic voltammetry (CV) at 600 °C. With an acceptable solubility and a relatively positive reduction potential of solute Cr^{3+}, the electrolytic reduction of chromium in FLiNaK-CrF₃ melt was performed on a tungsten electrode by potentiostatic electrolysis. After electrolysis for 21.5 h, the Cr^{3+} in the melt was effectively removed as confirmed by ICP-OES and CV. Then, the solubility of Cr_2O_3 in FLiNaK with ZrF₄ additive was analyzed by CV. The results showed that the solubility of Cr_2O_3 was greatly promoted by ZrF₄ and the reduction potential of zirconium is far more negative than that of chromium, which makes the electrolysis of chromium from Cr_2O_3 material possible. Thus, the electrolytic reduction of Cr in a FLiNaK-Cr₂O₃-ZrF₄ system was further performed by potentiostatic electrolysis on a nickel electrode. After electrolysis for 5 h, a thin layer of chromium metal (with a thickness of c.a. 20 μm) was deposited on the electrode, as confirmed by SEM-EDS and XRD techniques. This study verified the feasibility of electroextraction of Cr from the FLiNaK-CrF₃ and FLiNaK-Cr₂O₃-ZrF₄ molten salt systems.

1. Introduction

Molten fluorides are particularly appropriate as the coolant of molten salt reactors (MSR) because of their excellent heat transfer properties.[1–3] However, the oxidizing impurities contained in fluoride salts,[4] including adsorbed H_2O, dissolved HF, and metal impurity ions (Fe^{2+}, Ni^{2+}) are corrosive to structural materials,[5–8] particularly to the most vulnerable element Cr in those materials [eqn (1)–(4)].[9–11] The corrosion reactions lead to dissolution of Cr into the molten salt. Despite this problem, high temperature Cr-bearing alloys, such as Hastelloy, still have been used in molten fluorides because of their acceptable, time-tested, and overall high temperature properties.[12,13]

$$H_2O + 2F^- \rightarrow 2HF + O^{2-} \tag{1}$$

$$2Cr + 6HF \rightarrow 2CrF_3 + 3H_2 \tag{2}$$

$$2Cr + 3Fe^{2+} \rightarrow 2Cr^{3+} + 3Fe \tag{3}$$

$$2Cr + 3Ni^{2+} \rightarrow 2Cr^{3+} + 3Ni \tag{4}$$
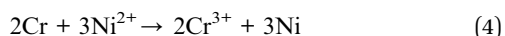
By periodic sampling and off-line chemical analysis, the Oak Ridge National Laboratory (ORNL)[14] found that chromium concentration was less than 150 ppm during the normal operation of molten salt reactor experiment (MSRE), and 70–80 ppm of chromium kept in molten fluorides will help to reduce the material corrosion. However, considering its neutron absorption, chromium needs to be removed when its concentration approaches to 300 ppm. Hence, developing a fast method to remove chromium in molten fluorides is necessary. The electrochemical methods are proposed to separate those impurities which have lower theoretical decomposition voltages than that of salt component. As one of the most important impurities in FLiNaK melt, Cr^{3+} in the form of CrF₃ presents a much lower theoretical decomposition voltage than LiF, NaF, and KF, thus it is supposed that Cr can be electrodeposited and separated from the FLiNaK-Cr^{3+} melts by electrolysis. Actually, the electrochemical behavior of Cr^{3+} in molten fluorides was widely studied. Our previous studies[4] found that the reduction of Cr^{3+} ions in molten FLiNaK was a two-step process by cyclic voltammetry (CV) and square wave voltammetry (SWV), namely, the initial Cr(III) reduction to Cr(II) followed by subsequent reduction to Cr. The first reduction step of Cr(III)/Cr(II) was reversible and the second reduction step of Cr(II)/Cr was quasi-reversible over the studied scan rates (0.05–0.4 V s⁻¹). Since the kinetics of chromium deposition in molten FLiNaK by electrochemical techniques is controlled by diffusion according to T. Yoko,[15] R. A. Bailey,[16] D. Ludwig,[17] and our previous studies.[4] Therefore, the most concern is that if Cr^{3+} ion can be efficiently removed from the melts by electrolytic reduction method and how long the process will take.

However, due to the hygrometric nature of fluorine salt and the pyro-hydrolysis of adsorbed water (eqn (1)), the oxide impurity (O^{2-}) in molten salt is unavoidable.[18–22] The Cr^{3+}

[a]Shanghai Institute of Applied Physics, Chinese Academy of Sciences, Shanghai 201800, PR China. E-mail: penghao@sinap.ac.cn; Fax: +86 021 39194053; Tel: +86 021 39194053

[b]Shanghai Institute of Optics and Fine Mechanics, Chinese Academy of Sciences, Shanghai 201800, PR China. E-mail: jiangfangling@siom.ac.cn; Fax: +86 021 69918204; Tel: +86 021 69918204

exhibits a high sensitivity towards O^{2-} ions and the interaction between the two would probably produce solid oxide compound (*e.g.* Cr_2O_3) with high melting point and low solubility. Therefore, the Cr^{3+} impurity in molten fluorides should generally exist in two forms: chromium(III) fluoride (*e.g.* CrF_3) and chromium(III) oxide (*e.g.* Cr_2O_3).

With the purpose of Cr^{3+} removal, electrolysis of chromium from both the CrF_3 and Cr_2O_3 raw materials should be performed. The reported high solubility of CrF_3[4,15–17] in molten FLiNaK makes its electrolysis feasible. However, with respect to the FLiNaK-Cr_2O_3 system, the solubility of Cr_2O_3 in FLiNaK is a key factor affecting chromium electroextraction. Our previous investigation and related reports[23–25] pointed out that the Cr_2O_3 solubility in molten fluorides was relatively low. For example, the solubility of Cr_2O_3 in molten FLiNaK and FLiBe at 600 °C was as low as 122 ppm and 183 ppm, respectively,[23] which makes the electrolysis difficult and challenging. Therefore, it is necessary to find suitable additives to increase Cr_2O_3 solubility in molten fluorides. ZrF_4 might be a good choice, which has a strong affinity towards oxide. Peng and Shen *et al.*[19,21,26] found that $Zr(IV)$ could readily combine with O^{2-} to produce zirconium oxide (*e.g.* ZrO_2) or zirconium oxy-fluoride species (*e.g.* $ZrOF_2$ and $Zr_2OF_{10}^{4-}$) in FLiNaK and FLiBe molten fluoride systems.[16,17] Besides, Gibilaro *et al.*[27] also found the interactions between Zr^{4+} and O^{2-} in LiF–CaF₂ would lead to the formation of ZrO_2 and $ZrO_{1.3}F_{1.4}$. These studies confirmed that ZrF_4 is a good oxide collector that can easily capture O^{2-} in molten fluorides.

Therefore, it is reasonably supposed that ZrF_4 can improve the solubility of solid oxides in melt through the reaction of $Zr(IV)$ and oxygen in these oxides. Song *et al.*[23] studied the dissolution behavior of Cr_2O_3 in various molten fluorides by combining electrochemical and chemical methods (including CV, ICP-OES, Raman, and XRD techniques), and found that the ZrF_4 additive significantly increased the solubility of Cr_2O_3 by 19 and 2 times in FLiNaK and FLiBe molten fluoride salts, respectively, with yielding the dissolution product of Cr^{3+} and $[ZrO_xF_y]^{4-2x-y}$ complex species through the dissolution mechanism of $Cr_2O_3 + ZrF_4 + F^- \rightarrow CrF_3 + ZrO_xF_y^{4-2x-y}$. Specifically, the solubility of Cr_2O_3 increased from 122 ppm to 2300 ppm in FLiNaK and increased from 183 ppm to 320 ppm in FLiBe by ZrF_4 at 600 °C. Besides, Peng *et al.*[18–21] studied the dissolution–precipitation behaviors of UO_2 in FLiNaK and FLiBe with ZrF_4 additive, and found that ZrF_4 can greatly improve the solubility of UO_2 in both systems. Particularly, their results showed that the maximum solubility of UO_2 in FLiNaK was increased by *a* factor of 5.76 when the added ZrF_4 concentration was up to 2.91 wt%, and UO_2 was dissolved as UOF_2 and $ZrOF_2$ species.[19] These studies demonstrated that ZrF_4 can effectively improve the solubility of oxides in molten fluorides. Moreover, ZrF_4 has a low neutron-absorption cross-section, which allows it to be used in the carrier media of MSR. Meanwhile, the theoretical decomposition potential difference between zirconium and chromium is significant. From the above, ZrF_4 is probably an ideal additive for improving the solubility of Cr_2O_3 in molten fluorides, which make the electrolysis of chromium from Cr_2O_3 material possible.

In this paper, with analysis of the reduction potentials of solute Cr^{3+} by cyclic voltammetry (CV), the feasibility of electrolyzing chromium from the FLiNaK-CrF_3 melt was verified. Then, the solubility of Cr_2O_3 in FLiNaK with ZrF_4 additive was analyzed by CV. The results showed that the solubility of Cr_2O_3 was greatly facilitated by ZrF_4, which make the electrolysis of chromium from this system possible. Furthermore, the electrolytic reduction of Cr in the FLiNaK-CrF_3 and FLiNaK-Cr_2O_3-ZrF_4 systems were performed by potentiostatic electrolysis on W and Ni electrodes, respectively. The removal rate of Cr^{3+} was examined by ICP-OES and CV, and the electrolytic product was characterized by SEM-EDS and XRD. The results showed that the Cr^{3+} in the melt was effectively removed after electrolysis of both systems. This study successfully verified the feasibility of electrolytic extraction of Cr from the FLiNaK-CrF_3 and FLiNaK-Cr_2O_3-ZrF_4 molten salt systems.

2. Experimental

2.1 Chemicals and molten salt systems

Before use, the highly-purified FLiNaK [LiF–NaF–KF (46.5 : 11.5 : 42 mol%)] eutectic salt was dehydrated by heating under vacuum from ambient temperature up to its melting point for 72 h. The main impurities contained in FLiNaK salt were analyzed by ICP-OES and shown in Table 1. Then, 300 g of dehydrated FLiNaK salt was weighed and loaded into a vitreous carbon crucible ($\Phi70\times H100$ mm). During the electrolysis experiment of FLiNaK-CrF_3 system, a certain amount of Cr^{3+} solute was introduced into FLiNaK salt in the form of CrF_3 (Sigma-Aldrich, 99.99%), and the electrolysis of Cr^{3+} was then conducted in this prepared FLiNaK-CrF_3 electrolyte, as shown in Fig. 1(a). While in the electrolysis of FLiNaK-Cr_2O_3-ZrF_4 system, an excess of Cr_2O_3 powder (*ca.* 10 g, Sigma-Aldrich, 99.9%) was added into FLiNaK salt, and the Cr_2O_3 ($\rho = 5.21$ g cm^{-3}) would deposited at the bottom of the molten bath ($\rho \approx 2$ g cm^{-3}) when balanced. Then a known amount of ZrF_4 (Sigma-Aldrich, 99.99%) was gradually introduced into the FLiNaK-Cr_2O_3 melt to promote the solubility of Cr_2O_3, and the electrolysis of Cr^{3+} by Cr_2O_3 dissolution was then conducted in this prepared FLiNaK-Cr_2O_3-ZrF_4 electrolyte, as shown in Fig. 1(b).

2.2 Chemical analysis

Concentrations of the solute chromium in molten fluoride electrolytes were determined by Inductively Coupled Plasma-Optical Emission Spectroscopy (ICP-OES) technique. Firstly, samples of the melt were siphoned by dipping a nickel tube ($\Phi6$

Table 1 The main impurities contained in the FLiNaK salt analyzed by ICP-OES

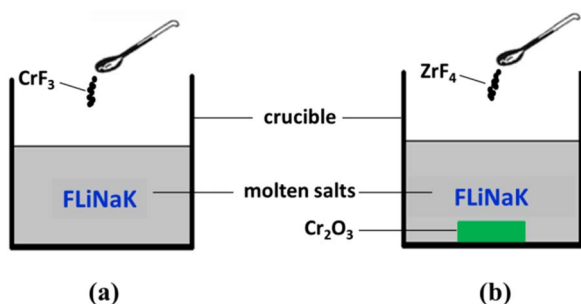| Impurities	Content/ppm
Fe	78
Cr	38
Ni	8
Ca	20
Mg	9
W	15

Fig. 1 Schematic diagram of the experimental systems for (a) FLiNaK-CrF_3 electrolysis and (b) FLiNaK-ZrF_4-Cr_2O_3 electrolysis.

mm) into the supernatant of the melt without touching the bottom precipitates. 0.1 g of finely pulverized sample was weighed-in a glove box. Then, the sample was dissolved in diluted 20% (v : v) HNO_3 and heated at 80 °C for ca. 30 min until the sample was completely dissolved. After cooling, the sample solution was transferred to a 50 ml flask and further diluted with deionized water. For each sample, duplicate decomposition tests of the sample were made. Chromium in the dissolved sample was then determined by Inductively Coupled Plasma-Optical Emission Spectroscopy (ICP-OES, Arcos, Spectro Co., Ltd). With the obtained results, we can compare the chromium content in the bath before and after electrolysis, and the removal efficiency of Cr is thus evaluated.

2.3 Electrochemical measurements

(1) Electrochemical analysis and apparatus. The crucible loaded with molten salts was transferred to a stainless steel cell inside an electric furnace. Then the salt was heated, melted, and kept at 600 °C for electrochemical measurements. The temperature was measured with a nickel–chromium thermocouple positioned just outside the crucible. The whole experiment was conducted in a glove box protected by dry argon gas atmosphere (99.999%), and the oxygen and moisture contents in the glove box were both strictly controlled below 0.5 ppm. The experimental apparatus used in present work has also been described in our previous studies.[4,18–22]

The electrochemical behaviors of CrF_3 and dissolved chromium species caused by Cr_2O_3 dissolution in molten fluorides with ZrF_4 additive were investigated by cyclic voltammetry (CV). The schematic diagram of the electrochemical set-up used in this study is shown in Fig. 2. The electrochemical cyclic voltammetry (CV) measurements were carried out with a three-electrode system connected to an electrochemical analyzer. A tungsten or nickel wire (1.0 mm diameter) was used as the working electrode; the surface area of this wire was determined by measuring the immersion depth in the melts after completion of the experiment. The auxiliary electrode was a graphite rod (6.0 mm diameter) with a large surface area (2.5 cm^2). The reference electrode was a platinum wire (1.0 mm diameter), which was proved to act as a quasi-reference electrode Pt/PtO$_x$/O^{2-}.[28,29] All potentials in this paper were measured with respect to this reference electrode and then transferred to vs. K/K$^+$
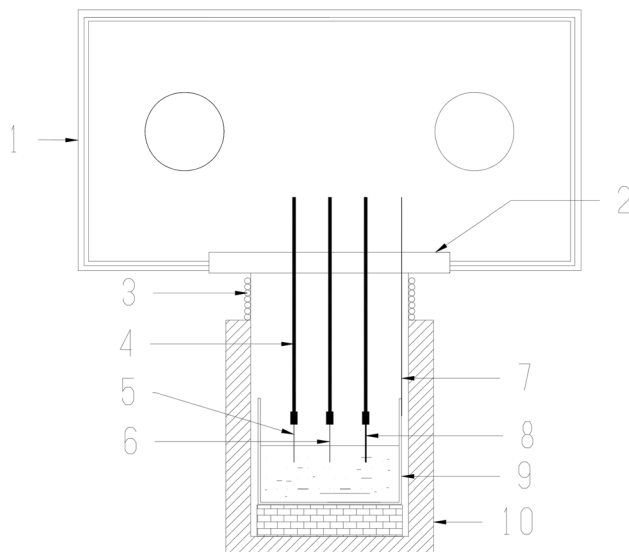

Fig. 2 Drawing of the electrochemical set-up used in this study. 1: Glove box. 2: Transition cover. 3: Water cooling coil let. 4: Alumina insulation tubes. 5: Working electrode. 6: Reference electrode. 7: Thermocouple. 8: Auxiliary electrode. 9: Vitreous carbon crucible and molten salt. 10: Electric furnace.

reference electrode according to literature.[30,31] An electrochemical analyzer, AUTOLAB (Ecochemie, NL), was used as the source of signal and for storage of data.

(2) Electrolysis and electrolysis products. During FLiNaK-CrF_3 electrolysis experiment, CrF_3 was the active component and electrolysis raw material. A potentiostatic mode was used for electrolysis. A tungsten wire (1.0 mm diameter) and graphite rod (spectral pure; 6.0 mm diameter) were employed as cathode and anode respectively, and the reference electrode was a platinum wire (1.0 mm diameter). The applied electrolytic potential was controlled at a constant value of 1.0 V vs. K/K$^+$ in the whole electrolysis process.

During FLiNaK-ZrF_4-Cr_2O_3 electrolysis experiment, Cr_2O_3 was the active component and electrolysis raw material. A potentiostatic mode was used for electrolysis. The cathode and anode were Ni plate (1.5 cm × 2.0 cm) and graphite rod (spectral pure; 6.0 mm diameter), respectively. And the reference electrode was a platinum wire (1.0 mm diameter) as well. A constant potential of 1.0 V vs. K/K$^+$ was used in the potentiostatic mode.

After electrolysis, the cathodic deposits were characterized by the techniques of X-ray diffraction (XRD; DY3614, PANzlytical Co., Ltd) and scanning electron microscopy (SEM; Merlin compact-60-83) equipped with an energy dispersive X-ray spectroscope (EDS).

3. Results and discussion

3.1 Electrochemical behavior of Cr^{3+} in FLiNaK melt

The typical cyclic voltammograms obtained on a W electrode in FLiNaK melt at 600 °C after addition of 345.30 ppm Cr^{3+} is shown in Fig. 3(a). Evidently, one couple of cathodic/anodic
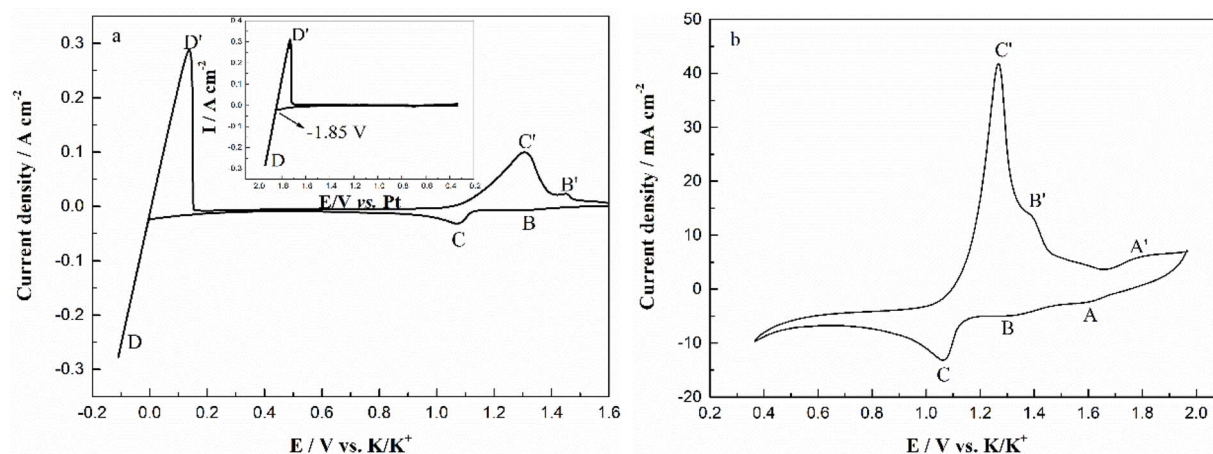
Fig. 3 (a) CV of the FLiNaK-CrF$_3$ (345.30 ppm Cr^{3+}) melt in the potential range of 1.60 V to −0.10 V vs. K/K$^+$. Inset: CV of the blank FLiNaK melt. (b) CV of the same FLiNaK-CrF$_3$ melt in the potential range of 1.90 V to 0.40 V vs. K/K$^+$. Working El.: W (S = 1.13 cm^2); auxiliary El.: graphite; reference El.: Pt; temperature: 600 °C; scan rate: 0.1 V s^{-1}.

signals D and D′ corresponding to the deposition and dissolution of one of the melt components can be observed. According to heats of formation data for fluorides given by Baes[32] and the investigation of Gabriela,[31] it can be presumed that the signal D corresponds to the electrodeposition of potassium, while the oxidation signal D′ is attributed to the dissolution of potassium (KF → K, 4.97 V vs. F$_2$/F$^-$; NaF → Na 5.03 V vs. F$_2$/F$^-$; LiF → Li, 5.52 V vs. F$_2$/F$^-$ at 600 °C). The reduction signal D at −1.85 V vs. Pt is shown in inset from Fig. 3(a). Thus, all potentials referenced to a platinum wire can be converted to vs. K/K$^+$. Besides the couple of D and D′, two reduction peaks B and C at 1.27 V and 1.07 V vs. K/K$^+$ in the cathodic run and two anodic counter-peaks B′ and C′ at 1.45 V and 1.31 V vs. K/K$^+$ can be observed.

In order to exhibit the details of the redox signals, Fig. 3(b) shows the cyclic voltammogram of the same FLiNaK-Cr^{3+} (345.30 ppm) melt on a W electrode in a relatively narrow potential range (from 1.90 V to 0.40 V vs. K/K$^+$) also at 600 °C and scan rate of 0.1 V s^{-1}. In this figure, the two reduction peaks B (1.27 V vs. K/K$^+$) and C (1.07 V vs. K/K$^+$), as well as their counter-oxidation peaks B′ (1.45 V vs. K/K$^+$) and C′ (1.31 V vs. K/K$^+$) also can be clearly observed. Since the deposition potential of Cr is more positive than that of alkali metal in a fluoride system and the peak current density for B and C linearly increases with the Cr^{3+} concentration (see Fig. 4), the observed peaks B and C should be attributed to the reduction of Cr^{3+}. According to our previous studies and other relevant reports, the reduction of Cr^{3+} in molten fluorides proceeds in two steps: the first reduction of Cr^{3+} to Cr^{2+} and the subsequent reduction of Cr^{2+} to metal Cr, denoted as B and C shown in eqn (5) and (6), respectively. What is worth mentioning, except for B/B′ and C/C′ couples, a new weak reduction signal A at around 1.60 V vs. K/K$^+$ associated with its counter-anodic signal A′ (1.80 V vs. K/K$^+$) can be observed in Fig. 3(b). Its peak current density is constant even if the concentration of Cr^{3+} increases. Thus, it is probably linked to the impurity Fe contained in the original FLiNaK eutectics (see Table 1). The attribution of the redox couple A/A′ will be discussed later.

$$\text{Peak B: } Cr^{3+} + e^- \rightarrow Cr^{2+} \tag{5}$$

$$\text{Peak C: } Cr^{2+} + 2e^- \rightarrow Cr \tag{6}$$
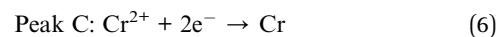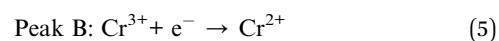
3.2 Electrolysis removal of Cr^{3+} from FLiNaK-CrF$_3$ melt

According to the theory of A. J. Bard,[33] the minimum potential difference for successful quantitative separation was considered to be 200 mV. From above analysis, the potential difference between Cr^{3+} and alkaline ions is approximately equal to 1.3 V, indicating that the Cr^{3+} can be theoretically removed from FLiNaK melt by potentiostatic electrolysis. Thus, potentiostatic electrolysis of the FLiNaK-CrF$_3$ system was carried out. After electrolysis, the system was on-line sampled at 600 °C and the concentration of Cr^{3+} remaining in melt was analyzed by ICP-OES.
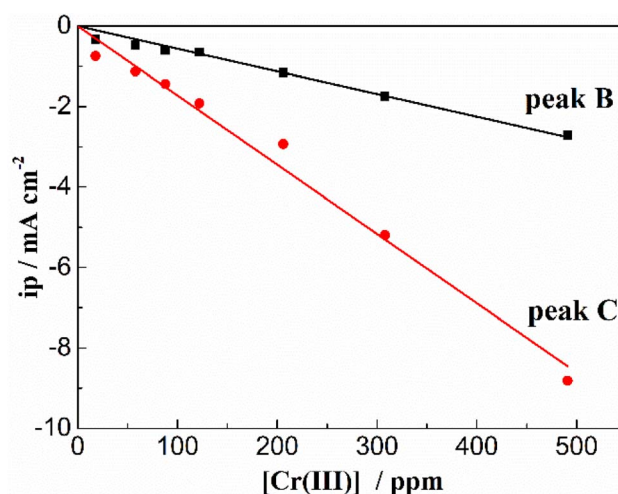

Fig. 4 Linear relationship between the peak current density and the Cr^{3+} concentration in FLiNaK melt at 600 °C at the scan rate of 0.1 V s^{-1} for both cathodic peak A and B. Working El.: W (S = 1.13 cm^2); auxiliary El.: graphite; reference El. Pt.
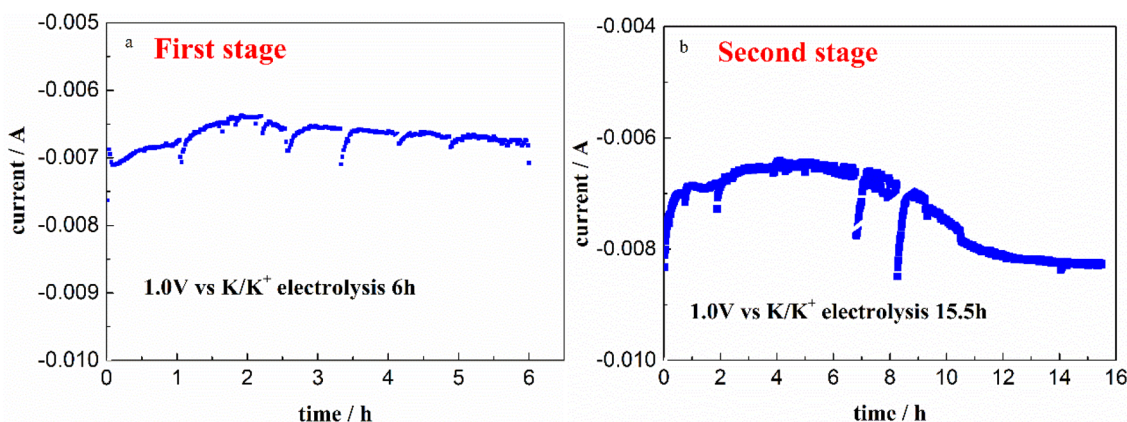
Fig. 5 Variations of the current on W cathode during the electrolysis at 1.0 V *vs.* K/K$^+$ and 600 °C for both two stages in FLiNaK-Cr^{3+} (345.30 ppm) melt. (a): The first stage; (b): the second stage. Working El.: W (S = 1.13 cm^2); auxiliary El.: spectral pure graphite; reference El. Pt.

3.2.1 First stage electrolysis. The current response *vs.* electrolysis time on a W electrode at 1.0 V *vs.* K/K$^+$ in FLiNaK-Cr^{3+} (345.30 ppm) melt for successive electrolysis of 6 h was recorded and shown in Fig. 5(a). The current decreased from −7 mA to −6.4 mA in the first 2 h, and then gradually increased to −6.6 mA for the following 4 h. Stable and continuous current output indicates that the Cr^{3+} ions are continuously being electrodeposited. After electrolysis, the remaining Cr^{3+} decreased from the initial 345.30 ppm to 108.61 ppm, which was analyzed by ICP-OES. That means, the decrement of Cr^{3+} was 236.69 ppm, as shown in Table 2. It is reasonable to speculate that the Cr^{3+} can be successfully removed by electrochemical reduction. However, the remaining Cr^{3+} content was still high as 108.61 ppm after this time of electrolysis for 6 h.

3.2.2 Second stage electrolysis. In order to further decrease the Cr^{3+} concentration, continual electrolysis was carried out on a W electrode at 1.0 V *vs.* K/K$^+$ for another 15.5 h. The relation between current and electrolysis time was given in Fig. 5(b). The current decreased from 8 mA to 6.5 mA in the first 3 h, then gradually increased to 8 mA in the following 8 h and eventually reached a plateau. After electrolysis for 15.5 h, the remaining Cr^{3+} further decreased from 108.61 ppm to 13.12 ppm. That means, the decrement of Cr^{3+} in this electrolysis stage was 95.49 ppm, as shown in Table 2.

Therefore, after the whole electrolysis of 21.5 h, the Cr^{3+} in melt successfully decreased from the initial 345.30 ppm to a sufficiently low concentration level of 13.12 ppm, with the practical removal content of 332.18 ppm (Table 2). This result confirmed that the Cr^{3+} in melt can be almost removed through electrolysis method. Besides, it should be noted that the

impurity Fe ions in molten FLiNaK analyzed by ICP-OES also continuously decreased from 78.19 ppm to below the detection limit after the overall electrolysis duration for 21.5 h. This result indicates that a certain amount of charges were used for Fe deposition. The current fluctuation in electrolytic process may be caused by the absorption and desorption of the electrodeposited products, resulting in a change in the electrode surface area.

According to the CV theory, the peak current density of the electroactive solute (in this case the Cr^{3+}) is fundamentally proportional to its concentration for an electrode process controlled by diffusion (Fig. 5). Thus, the variation of the Cr^{3+} concentration remaining in the melts can be monitored by CV measurements throughout the electrolysis process. Fig. 6 shows the cyclic voltammograms of FLiNaK-Cr^{3+} melts before electrolysis, after 6 h and 21.5 h electrolysis on W cathode at 1.0 V *vs.* K/K$^+$. Obviously, the reduction peak current density of Cr^{3+} (Cr^{3+}/Cr^{2+} reduction for peak B and Cr^{2+}/Cr reduction for peak C) gradually decreased as the electrolysis progressed, and eventually no reduction peak current density can be detected on cyclic voltammogram after electrolysis for 21.5 h. This result indicates a decreasing Cr^{3+} concentration during electrolysis and until it drops to below the detection limit of CV, which agreed well with the result obtained from ICP-OES. It should be noted that the cathodic peak A attributed to Fe reduction also decreased after electrolysis, indicating the trace impurity of Fe ions was electrochemically removed as well. Therefore, the reduction peak A corresponds to the reduction of Fe^{2+} to iron metal (Fe^{2+} + 2e$^-$ → Fe), and the oxidation peak A′ corresponds to the oxidation of Fe metal to iron ions (Fe − 2e$^-$ → Fe^{2+}).

Table 2 The concentration of Cr in FLiNaK melt before and after electrolysis

Samples	Before electrolysis	Electrolysis for 6 h	Electrolysis for 21.5 h
Electrolysis potential (V)	—	1.0 *vs.* K/K$^+$	1.0 *vs.* K/K$^+$
Cr concentration in melt analyzed by ICP-OES (ppm)	345.30	108.61	13.12
Cr practical removal content analyzed by ICP-OES (ppm)	—	236.69	332.18
Fe concentration analyzed by ICP-OES (ppm)	78.19	7.43	<−0.04

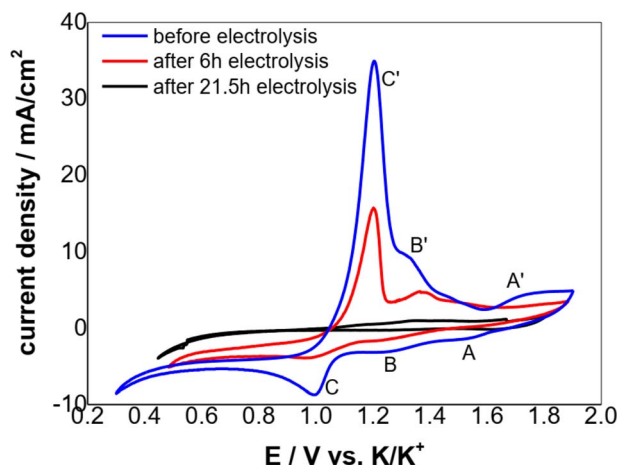**Fig. 6** Typical CVs of the FLiNaK-Cr^{3+} (345.30 ppm) melts before and after electrolysis on W cathode at 600 °C. Scan rate: 0.1 V s^{-1}; working El.: W ($S = 1.13$ cm^2); auxiliary El.: graphite; reference El. Pt.

3.3 Solubility of Cr_2O_3 in molten FLiNaK with ZrF_4 additive

3.3.1 Solubility of Cr_2O_3 in pure FLiNaK melt.
The solubility of Cr_2O_3 in molten FLiNaK was firstly studied by cyclic voltammetry method. The cyclic voltammograms of FLiNaK and FLiNaK-Cr_2O_3 systems were measured on tungsten electrode at 600 °C with scan rate of 0.1 V s^{-1}, and overlap of the two results were presented in Fig. 7. Obviously, only one couple of cathodic/anodic signals D and D′ corresponding to the deposition and dissolution of K was observed in the pure FLiNaK (dotted black line). After addition of Cr_2O_3 into FLiNaK melts, the voltammogram of the system on tungsten electrode was featureless (solid red line). No reduction and oxidation signals or processes can be detected prior to the deposition of potassium metal (signal D), and the obtained CV curve is almost the same as that in the pure FLiNaK melt. The similarity of the CVs between FLiNaK and FLiNaK-Cr_2O_3 systems indicates that the solubility of Cr_2O_3 in FLiNaK was low enough that the dissolved

chromium species cannot be detected by CV. Actually, the accurate value of Cr_2O_3 solubility in FLiNaK was determined to be 122 ppm at 600 °C through dissolved chromium content determination (83 ppm Cr^{3+}) by chemical analysis (ICP-OES).[23] Herein, the electrochemical CV results agreed well with that obtained by ICP-OES, and both techniques revealed that the solubility of Cr_2O_3 in the FLiNaK melt is quite low (122 ppm).

3.3.2 Solubility of Cr_2O_3 in FLiNaK-ZrF_4 melt.
After addition of 2.14 wt% ZrF_4 into FLiNaK-Cr_2O_3 melts, the cyclic voltammogram of FLiNaK-Cr_2O_3-ZrF_4 (2.14 wt%) was measured on W electrode and the result was shown as dotted red line in Fig. 8. Besides one couple of cathodic/anodic signals D and D′ corresponding to the deposition and dissolution of potassium metal, three reduction peaks, B, C and R at 1.27, 1.07 V and 0.24 V vs. K/K$^+$, respectively, in the cathodic run can be observed. Obviously, the locations of the peaks B and C are consistent with that obtained in FLiNaK-CrF_3 melt (solid black line), also with a potential difference of ∼0.2 V. Thus, the two peaks B and C in this case corresponded to the reductions of Cr^{3+}/Cr^{2+} and Cr^{2+}/Cr, respectively. The same nature of the two peaks B and C in FLiNaK-CrF_3 and FLiNaK-ZrF_4-Cr_2O_3 systems proves that Cr_2O_3 dissolves into molten salt in the form of CrF_3 species. This result indicated the dissolution mechanism of Cr_2O_3 in FLiNaK-ZrF_4 melt was attributed to the reaction between ZrF_4 and oxygen in Cr_2O_3, with releasing Cr^{3+} as the form of CrF_3 that dissolves into molten salt. Moreover, compared with the FLiNaK-Cr_2O_3 system, the CV curve in FLiNaK-ZrF_4-Cr_2O_3 showed a significant current enhancement for peaks B (Cr^{3+}/Cr^{2+}) and C (Cr^{2+}/Cr). Hence, it can be concluded that the solubility of Cr_2O_3 in FLiNaK melt was greatly facilitated by ZrF_4 addition, and the Cr_2O_3 was dissolved as the form of CrF_3, which was consistent with that reported by Song et al.[23] In fact, Song et al.[23] proved that the dissolution product of Cr_2O_3 in molten FLiNaK-ZrF_4 system corresponded to CrF_3 and Zr(IV) oxyfluoride through the reaction of $Cr_2O_3 + ZrF_4 + F^- \rightarrow CrF_3 + ZrO_xF_y^{4-2x-y}$, as determined by XRD technique and chemical analysis. It should be noted that, the newly appeared peak R at
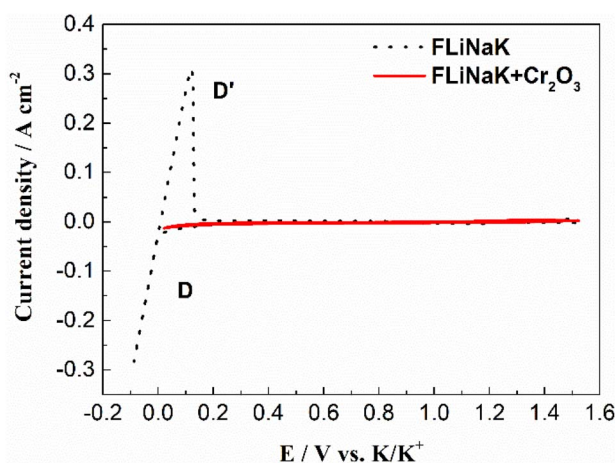

Fig. 7 CVs of FLiNaK and FLiNaK-Cr_2O_3 systems at 600 °C and scan rate of 0.1 V s^{-1}. Working El.: W ($S = 1.13$ cm^2); auxiliary El.: graphite; reference El.: Pt.
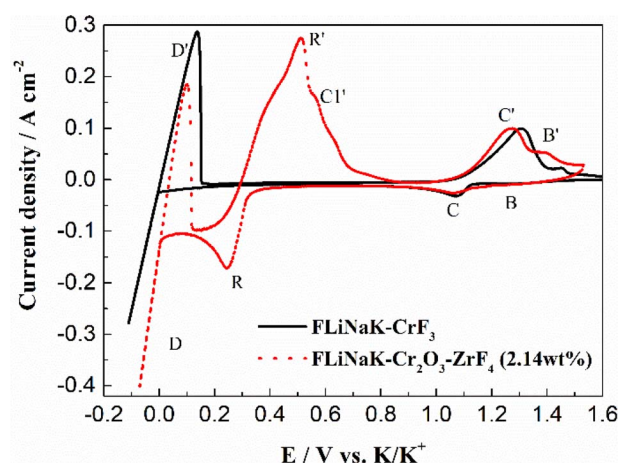

Fig. 8 The CVs of FLiNaK-CrF_3 and FLiNaK-ZrF_4-Cr_2O_3 melt at 600 °C and scan rate of 0.1 V s^{-1}. Working El.: W ($S = 1.13$ cm^2); auxiliary El.: graphite; reference El.: Pt.
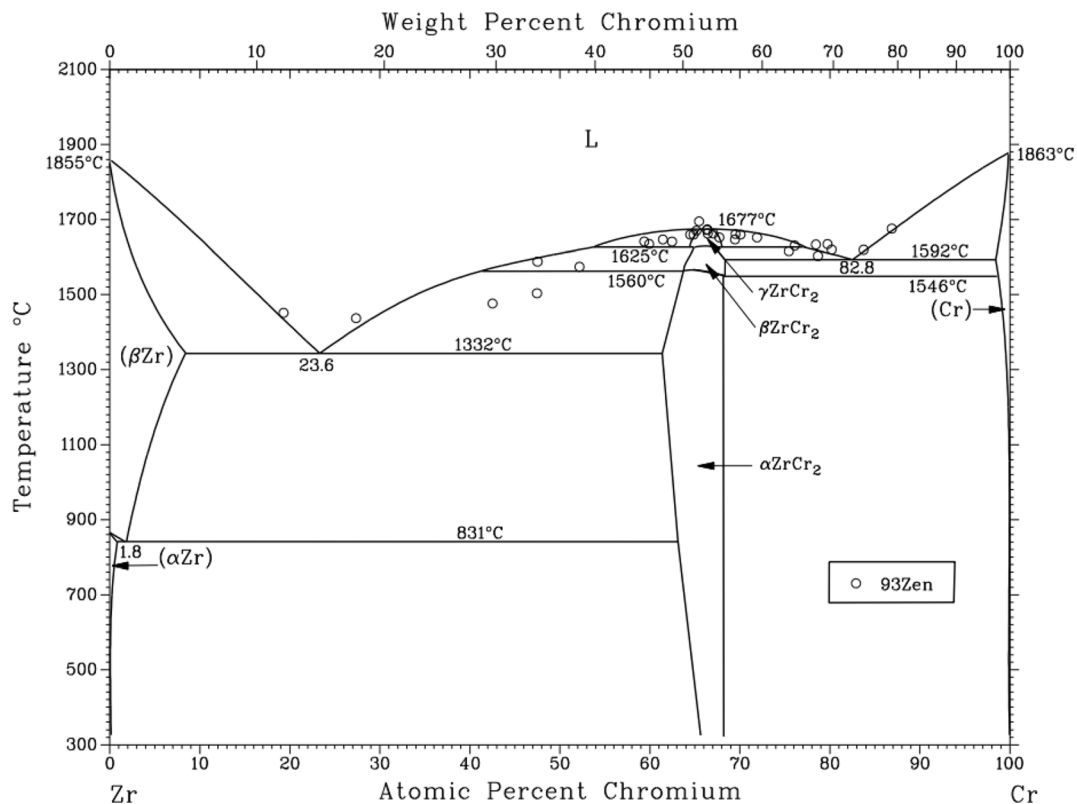
Fig. 9 Cr–Zr binary phase diagram.

0.24 V *vs.* K/K$^+$ should be attributed to the reduction of Zr^{4+}/Zr with a four-electron exchanging process[27] since the deposition potential of zirconium is more negative than that of chromium metal in a fluoride system. The anode signal R′ corresponding to the dissolution of Zr metal. Besides, according to the Cr–Zr binary phase diagram (Fig. 9), it is easy to form intermetallic compounds or alloys between chromium and zirconium metals. Thus, the signal C1′ should be arised from the dissolution of Zr–

Cr alloys formed in the cathodic run. The obtained CV results in present study was highly consistent with that reported by Song *et al.*[23] in the same system (FLiNaK–ZrF$_4$–Cr$_2$O$_3$).

It should be noted that, although Song *et al.*[23] also studied the electrochemical behavior of the FLiNaK–ZrF$_4$–Cr$_2$O$_3$ system, they only focused on the attribution of peaks at a single concentration, and did not systematically study the electrochemical law at different ZrF$_4$ concentrations. Meanwhile, ref.
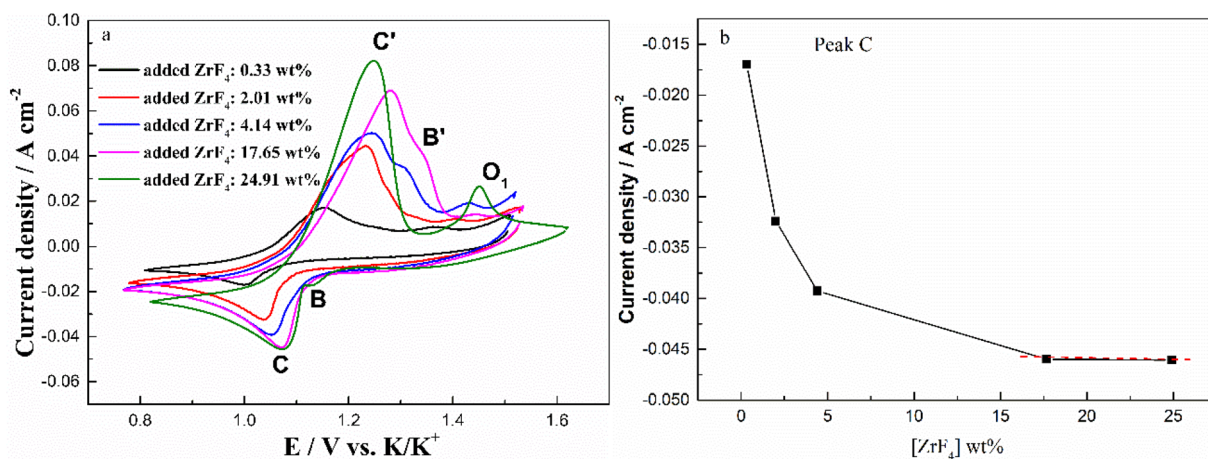

Fig. 10 (a) Typical CVs recorded on a tungsten electrode in the FLiNaK–Cr$_2$O$_3$ melt with different concentrations of added ZrF$_4$ at 600 °C and scan rate of 0.1 V s^{-1}. Working El.: W ($S = 1.13$ cm^2); Auxiliary El.: graphite; reference El.: Pt. (b) ZrF$_4$ concentration *vs.* peak current density (peak C).
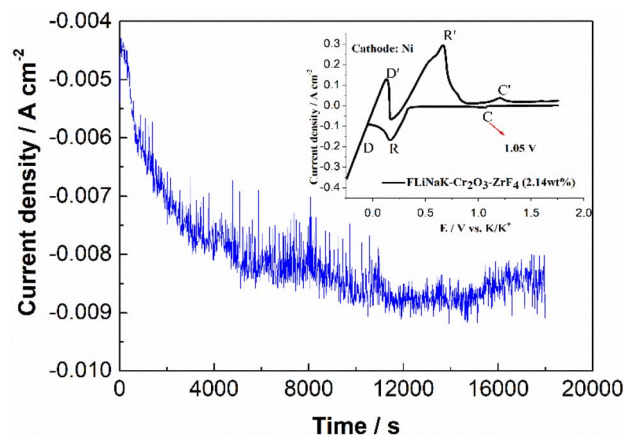
Fig. 11 Current-variation curve during the potentiostatic electrolysis of FLiNaK-Cr_2O_3-ZrF_4 (17.65 wt%) system at 1.0 V (vs. K/K$^+$) and 600 °C on Ni electrode. Inset: CV of FLiNaK-ZrF_4-Cr_2O_3 melt at 600 °C and scan rate of 0.1 V s^{-1}. Working El.: Ni; auxiliary El.: graphite; reference El.: Pt.

23 did not focus on the electrolytic removal of chromium. Therefore, the electrochemical measurement of FLiNaK-Cr_2O_3 under different ZrF_4 conditions and the further electrolytic extraction of chromium will be studied subsequently.

To further investigate the effect of ZrF_4 concentration on the solubility of Cr_2O_3, the cyclic voltammograms of FLiNaK-Cr_2O_3 melt with different concentrations of ZrF_4 were recorded and the results were shown in Fig. 10(a). As can be seen in Fig. 10(a), the current densities of reduction peaks B (Cr^{3+}/Cr^{2+}) and C (Cr^{2+}/Cr) both gradually increased with ZrF_4 additions. When the concentration of ZrF_4 increased from 0.33 to 4.14 wt%, the reduction current density of peak C assigned to the reduction of Cr^{2+} to Cr distinctively increased from 0.016 to 0.044 A cm^{-2}, while the reduction current density of B for Cr^{3+} to Cr^{2+} increased from 0.004 to 0.009 A cm^{-2}. This result implied that the dissolved chromium ions caused by Cr_2O_3 dissolution gradually increased with ZrF_4 additions, since the peak current density is proportional to the concentration of the electroactive species.

In addition to the redox peaks B/B′ and C/C′, a new oxidation peak O_1 appeared (within the potential range 1.35–1.50 V vs. K/K$^+$). The formation of oxidation peak O_1 may be related to the formation of zirconium oxy-fluoride species in the FLiNaK-ZrF_4-Cr_2O_3 melt. Previous studies[19,21,23,26] also confirmed the existence of stable Zr(IV) oxy-fluoride species in molten fluoride media. The reasons for the formation of zirconium oxy-fluoride have been described in detail in previous text. Moreover, it was found that as the concentration of ZrF_4 increased, the oxidation peak O_1 current gradually increased, indicating that the concentration of the formed zirconium oxy-fluoride species also gradually increased.

Fig. 10(b) shows the relationship between the added ZrF_4 concentration and peak current density (peak C). It can be clearly observed that the peak current density of Cr^{2+} to Cr gradually increases with the addition of ZrF_4. When ZrF_4 increases to 17.65 wt% and 24.91 wt%, the curve approaches the plateau as shown in Fig. 10(b). These observations indicate that ZrF_4 can promote solubility of Cr_2O_3 in FLiNaK to a certain extent, and its maximum solubility can be achieved when the added concentration of ZrF_4 corresponded to 17.65 wt%.

It should be noted that the solubility of Cr_2O_3 in molten FLiNaK with ZrF_4 additive has already been determined by ICP-OES, as reported by Song et al.[23] Actually, they found that the specific value of Cr_2O_3 solubility in FLiNaK can greatly increase from 122 ppm to 2300 ppm level (by 19 times) through ZrF_4 additive, which agreed well with the results obtained by electrochemical analysis in case of present study. Besides, the theoretical decomposition voltage of zirconium is far more negative than that of chromium, and in this case the potential difference between Cr^{2+}/Cr and Zr^{4+}/Zr reductions is 0.83 V vs. K/K$^+$, which is much larger than the minimum value of 200 mV required for electrolytic separation. Therefore, it is feasible to electrolyze chromium with Cr_2O_3 raw material from FLiNaK-ZrF_4 melt.

3.4 Electrolysis of chromium from molten FLiNaK-ZrF_4-Cr_2O_3 system

The CV of FLiNaK-Cr_2O_3-ZrF_4 (2.14 wt%) was measured on Ni electrode at 600 °C, as shown in inset from Fig. 11. Compared
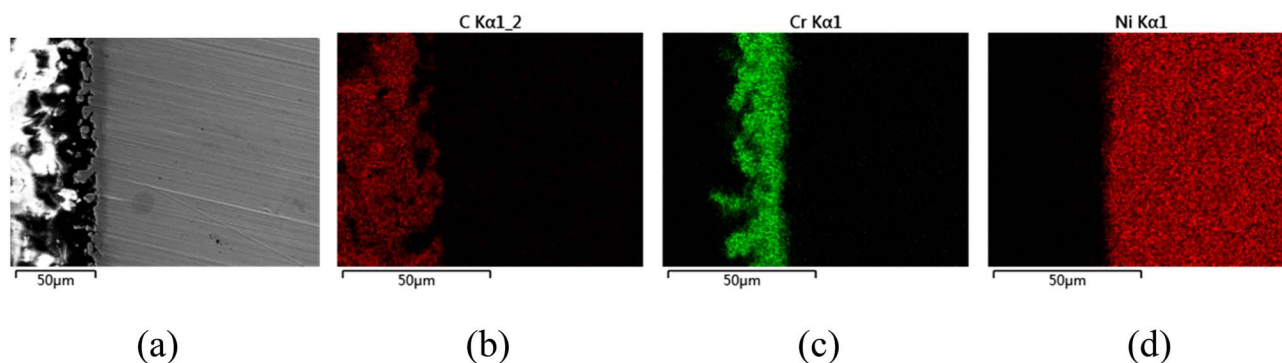

Fig. 12 (a) SEM photo of the cross-section of the cathodic deposits obtained by potentiostatic electrolysis at 1.0 V (vs. K/K$^+$) on a Ni electrode in FLiNaK-Cr_2O_3-ZrF_4 (17.65 wt%) system for 5 h at 600 °C. (b), (c), and (d) the corresponding EDS mapping patterns images for C (from the SEM inlay material: epoxy resin), Cr (electrolytic product) and Ni (cathode substrate) elements analysis.
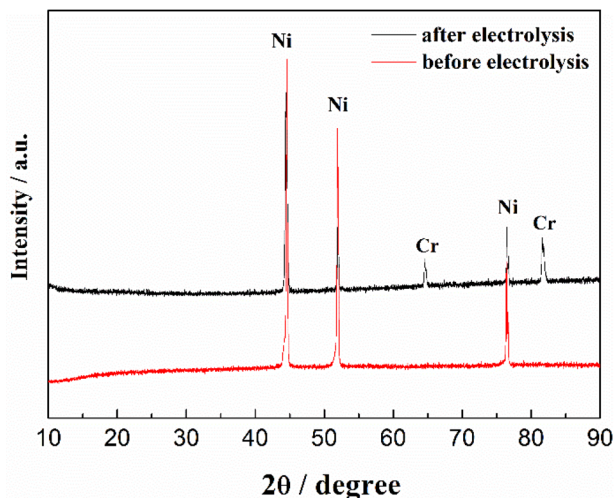
Fig. 13 XRD pattern of the cathodic deposits in FLiNaK-Cr_2O_3-ZrF_4 (17.65 wt%) system on Ni electrode. Red line: pure substrate of Ni electrode before electrolysis; black line: Ni electrode with cathodic deposits (Cr metal) after electrolysis.

with the W electrode, the signal of Cr^{2+} reduction to metallic Cr can still be observed on the Ni electrode, and the potential is basically consistent at 1.05 V *vs.* K/K$^+$. Based on the analysis results in Fig. 8, 10 and inset (from Fig. 11), the potentiostatic electrolysis of FLiNaK-Cr_2O_3-ZrF_4 (17.65 wt%) system was further performed on a Ni plate at the constant potential of 1.0 V (*vs.* K/K$^+$) for 5 h. The current density varied in the range of 4–9 mA cm^{-2} in the whole electrolysis duration, as shown in Fig. 11. The time–current density curve fluctuates significantly, which possibly due to the continuous deposition of electrolytic products on the cathode Ni plate during the electrolysis process and a coating of uneven thickness is formed. After electrolysis, the electrode was cleaned, cut, embedded, polished, and the electro-deposits on Ni electrode were analyzed by SEM-EDS (Fig. 12(a–d)). The results showed that a chromium layer with the thickness of *ca.* 20 μm was formed and coated on the surface of Ni electrode, as shown in Fig. 12(c). XRD analysis further confirmed this layer corresponded to Cr metal (Fig. 13).

Potentiostatic electrolysis in FLiNaK-Cr_2O_3-ZrF_4 system can successfully produce Cr metal as the form of electro-deposited coating. These results prove the feasibility of electrolyzing chromium from Cr_2O_3 raw materials in molten fluorides containing ZrF_4, and thus achieving the goal of chromium extraction.

4. Conclusion

The electrochemical behavior of Cr^{3+} was studied in the FLiNaK melts using W electrode at 600 °C by cyclic voltammetry. For a W electrode, the reduction of CrF_3 in FLiNaK melts is two steps reaction: $Cr^{3+} + e^- \rightarrow Cr^{2+}$ and $Cr^{2+} + 2e^- \rightarrow Cr$. Then, potentiostatic electrolysis of Cr in the FLiNaK-CrF_3 melt was performed on W electrode for 21.5 h. The ICP-OES results showed that Cr^{3+} in melt decreased from the initial 345.30 ppm to 13.12 ppm, indicating an effective removal of Cr^{3+} with the

practical removal content of 332.18 ppm. Moreover, the CV results showed a gradual decrease of reduction peak current for Cr^{3+} during electrolysis, and the reduction peaks B (Cr^{3+}/Cr^{2+}) and C (Cr^{2+}/Cr) almost could not be detected by cyclic voltammetry after electrolysis. This result indicates a decreasing Cr^{3+} concentration and until to below the detection limit of CV.

The CV of FLiNaK-Cr_2O_3 system was similar with that of blank FLiNaK, indicating that the solubility of Cr_2O_3 is quite low in FLiNaK melt. The electrochemical behavior of Cr_2O_3 after adding ZrF_4 was studied in FLiNaK molten salt system on W electrode at 600 °C by cyclic voltammetry. The reduction peak current of Cr^{3+} obviously increases with ZrF_4 addition, indicating that the solubility of Cr_2O_3 in FLiNaK can be greatly promoted by ZrF_4 additive. When the concentration of ZrF_4 added reaches 17.65 wt%, the solubility of Cr_2O_3 in FLiNaK salt reaches its maximum value. These results make the electro-extraction of Cr with Cr_2O_3 from ZrF_4-containing molten fluorides possible. Therefore, the potentiostatic electrolysis of FLiNaK-Cr_2O_3-ZrF_4 (17.65 wt%) system was further performed on a Ni plate at the constant potential of 1.0 V (*vs.* K/K$^+$) for 5 h. Characterization of the electrolytic product by SEM-EDS and XRD revealed that metallic Cr can be successfully obtained on the surface of Ni plate. This study verified the feasibility of electroextraction of Cr from CrF_3 and Cr_2O_3 in molten fluorides.

Conflicts of interest

There are no conflicts to declare.

Acknowledgements

References

1 M. Salanne, C. Simon, P. Turq and P. A. Madden, *J. Fluorine Chem.*, 2009, **130**, 38.

2 J. P. M. van der Meer and R. J. M. Konings, *J. Nucl. Mater.*, 2007, **360**, 16.

3 J. Krepel, B. Hombourger, C. Fiorina, K. Mikityuk, U. Rohde, S. Kliem and A. Pautz, *Ann. Nucl. Energy*, 2014, **64**, 380.

4 H. Peng, M. Shen, C. Y. Wang, T. Su, Y. Zuo and L. D. Xie, *RSC Adv.*, 2015, **5**, 76689.

5 S. Delpech, C. Cabet, C. Slim and G. S. Picard, *Mater. Today*, 2010, **13**, 34.

6 T. Nagasaka, M. Kondo, T. Muroga, N. Noda, A. Sagara, O. Motojima, A. Suzuki and T. Terai, *J. Nucl. Mater.*, 2009, **716**, 386.

7 M. Kondo, T. Nagasaka, A. Sagara, N. Noda, T. Muroga, Q. Xu, M. Nagura, A. Suzuki and T. Terai, *J. Nucl. Mater.*, 2009, **685**, 386.

8 M. Kondo, T. Nagasaka, Q. Xu, T. Muroga, A. Sagara, N. Noda, D. Ninomiya, M. Nagura, A. Suzuki, T. Terai and N. Fujii, *Fusion Eng. Des.*, 2009, **84**, 1081.

9 L. C. Olson, J. W. Ambrosek, K. Sridharan, M. H. Anderson and T. R. Allen, *J. Fluorine Chem.*, 2009, **130**, 67.

10 J. Qiu, Y. Zou, G. Yu, H. Liu, Y. Jia, Z. Li, P. Huai, X. Zhou and H. Xu, *J. Fluorine Chem.*, 2014, **168**, 69.

11 D. Williams, L. Toth and K. Clarno, in *ORNL/TM-2006/12*, 2006.

12 D. Williams, D. Wilson, J. Keiser, L. Toth and J. Caja, *Research on Molten Fluorides as High Temperature Heat Transfer Agents*, American Nuclear Society Winter Meeting, 2003.

13 H. E. McCoy, R. L. Beatty, W. H. Cook, R. E. Gehlbach, C. R. Kennedy, J. W. Koger, A. P. Litman, C. E. Sessions and J. R. Weir, *Nucl. Technol.*, 1970, **8**, 156.

14 ORNL, *Chemical aspect of MSRE operations*, 1971, **http://www.energyfromthorium.com/pdf/ORNL-4658.pdf**.

15 T. Yoko and R. A. Bailey, *J. Electrochem. Soc.*, 1984, **131**, 2590.

16 R. A. Bailey, *J. Appl. Electrochem.*, 1986, **16**, 737.

17 D. Ludwig, L. Olson, K. Sridharan, M. Anderson and T. Allen, *Corrosion Eng. Sci. Technol.*, 2011, **46**, 360.

18 H. Peng, M. Shen, Y. Zuo, X. X. Tang, R. Tang and L. D. Xie, *Electrochim. Acta*, 2016, **222**, 1528.

19 H. Peng, M. Shen, Y. Zuo, H. Y. Fu and L. D. Xie, *J. Nucl. Mater.*, 2018, **510**, 256.

20 H. Peng, W. Huang, L. D. Xie and Q. N. Li, *J. Nucl. Mater.*, 2020, **531**, 152004.

21 H. Peng, Y. L. Song, N. Ji, L. D. Xie, W. Huang and Y. Gong, *RSC Adv.*, 2021, **11**, 18708.

22 H. Peng, N. Ji, W. Huang and Y. Gong, *Int. J. Energy Res.*, 2023, **2023**, 4447405.

23 Y. L. Song, M. Shen, H. Peng, C. Y. Wang, S. F. Zhao, Y. Zuo and L. L. Xie, *J. Electrochem. Soc.*, 2020, **167**, 023501.

24 V. Danielik, P. Fellner, D. Sulekova and J. Thonstad, *J. Electrochem. Soc.*, 2012, **159**, C86.

25 D. Sulekova, V. Danielik, P. Fellner and J. Thonstad, *Metall. Mater. Trans. B*, 2013, **328**, 44B.

26 M. Shen, H. Peng, M. Ge, C. Y. Wang, Y. Zuo and L. D. Xie, *RSC Adv.*, 2015, **5**, 40708.

27 M. Gibilaro, L. Massot, P. Chamelot, L. Cassayre and P. Taxil, *Electrochim. Acta*, 2013, **95**, 185.

28 Y. Berghoute, A. Salmi and F. Lantelme, *J. Electroanal. Chem.*, 1994, **365**, 171.

29 A. D. Graves and D. Inman, *Nature*, 1965, **20**, 481.

30 H. Qiao, T. Nohira and Y. Ito, *Electrochim. Acta*, 2002, **47**, 4543.

31 G. Durán-Klie, D. Rodrigues and S. Delpech, *Electrochim. Acta*, 2016, **195**, 19.

32 C. F. Baes Jr., *J. Nucl. Mater.*, 1974, **51**, 149.

33 A. J. Bard and L. R. Faulkner, *Electrochemical Methods: Fundamentals and Applications*, Wiley, New York, 1980.